Article

Cryptophane nanoscale assemblies expand 129Xe NMR biosensing

Serge D. Zemerov, Benjamin W. Roose, Mara L Greenberg, Yanfei Wang, and Ivan J. Dmochowski

Anal. Chem., **Just Accepted Manuscript** • Publication Date (Web): 21 May 2018

Cryptophane nanoscale assemblies expand ^{129}Xe NMR biosensing

Serge D. Zemerov, Benjamin W. Roose, Mara L. Greenberg,[†] Yanfei Wang,[‡] and Ivan J. Dmochowski*

Department of Chemistry, University of Pennsylvania, 231 S 34th St., Philadelphia, PA 19104

ABSTRACT: Cryptophane-based biosensors are promising agents for the ultrasensitive detection of biomedically relevant targets *via* ^{129}Xe NMR. Dynamic light scattering revealed that cryptophanes form water-soluble aggregates of tens-to-hundreds of nanometers in size. Acridine orange fluorescence quenching assays allowed quantitation of aggregation state, with critical concentration ranging from 200 to 600 nM, depending on the cryptophane species in solution. Addition of excess carbonic anhydrase (CA) protein target to a benzenesulfonamide-functionalized cryptophane biosensor (C8B) led to C8B disaggregation and produced the expected 1:1 C8B-CA complex. C8B showed higher affinity at 298 K for the cytoplasmic isozyme CAII than the extracellular CAXII isozyme, a biomarker of cancer. Using hyper-CEST NMR, we explored the role of stoichiometry in detecting these two isozymes. At CA-saturating conditions, we observed that isozyme CAII produces a larger ^{129}Xe NMR chemical shift change (δ= 5.9 ppm, relative to free biosensor) than CAXII (δ= 2.7 ppm), which indicates the strong potential for isozyme-specific detection. However, stoichiometry-dependent chemical shift data indicated that biosensor disaggregation contributes to the observed ^{129}Xe NMR chemical shift change that is normally assigned to biosensor-target binding. Finally, we determined that monomeric cryptophane solutions improve hyper-CEST saturation contrast, which enables ultrasensitive detection of biosensor-protein complexes. These insights into cryptophane-solution behavior support further development of xenon biosensors, but will require reinterpretation of the data previously obtained for many water-soluble cryptophanes.

Molecules that self-assemble and exist in equilibrium with aggregates in solution are prominent in the literature, including complex salts, branched polymers, amyloid peptides, polymethine dyes, porphyrins, pi-conjugated macrocycles, fullerenes, and other large hydrophobic molecules.[1–7] Their supramolecular architectures remain challenging to design but are generally tuned by varying molecular concentration and amphiphilic character, solvent composition, and surfactant additives. Such aggregates have emergent properties for uses in drug delivery, sensing, and imaging. For example, a library of cyclodextrin derivatives[8,9] allowed encapsulation of the antimicrobial agent metronidazole[10] and the breast cancer drug tamoxifen.[11] Additionally, various organic compounds and biomolecules exhibit intense fluorescence in their aggregated state.[12–17] This aggregation-induced emission (AIE) has recently been used to identify cancer cells using a ratiometric fluorescent probe.[18] For many other molecules, however, spectroscopic signatures of aggregation are subtle, and may go undetected. We recently discovered water-soluble aggregates of cryptophanes, which are prototypal organic host molecules amenable to investigation by ^{129}Xe NMR spectroscopy (Figure 1). The characterization of cryptophane aggregation phenomena informs the use of such molecules for sensing applications, and further highlights the potential to form soluble aggregates with many drug-like molecules.

First synthesized in 1985 *via* the linkage of two cyclotribenzylene units by three ethylene linkers to give cryptophane-A,[19] many cryptophanes have since been generated by modifying the internal volume of the cage and the substituents attached to the aromatic rings.[20] Importantly, it was established in 1998 that cryptophane-A binds xenon with good affinity ($K_a \approx 3000$ M^{-1} in $C_2D_2Cl_4$ at 278 K) and an exchange rate that is sufficiently slow to obtain well-resolved signals *via* ^{129}Xe NMR.[21] This has motivated the investigation of cryptophanes as contrast agents for hyperpolarized (hp) ^{129}Xe magnetic resonance spectroscopy (MRS) and imaging (MRI) modalities, which have been shown to complement ^{1}H MRI for human lung and brain imaging.[22–25] The ^{129}Xe isotope is attractive for applications in biomolecular imaging due to its relatively high natural abundance of 26.4%,[26] solubility in many organic and aqueous solvents,[27] and large, polarizable electron cloud. Xenon's polarizability imparts affinity for void spaces as well as sensitivity to its molecular environment, resulting in a nearly 300 ppm ^{129}Xe NMR chemical shift window.[28] Moreover, hp ^{129}Xe, readily achieved by the process of spin-exchange optical pumping, can reach 10^4-10^8 signal enhancement over the thermally polarized Boltzmann population of nuclear spins.[29] These features have been exploited in the design of xenon biosensors that generate a unique ^{129}Xe NMR chemical shift or "turn on" signal[30–33] upon association with their target.

In 2001 the first xenon biosensor was developed through biotin-modification of cryptophane-A. Introduction of avidin in solution produced a ~3 ppm downfield hp ^{129}Xe NMR chemical shift.[34] This example has led our lab and others to synthesize cryptophane-based ^{129}Xe biosensors that report on proteins,[35–41] biothiols,[42] pH,[43,44] metal ions,[45–49] and DNA[50] *via* direct-detection ^{129}Xe NMR spectroscopy. To increase the potential for molecular imaging, the substantially more sensitive hyper-CEST NMR technique was developed, which combines hp ^{129}Xe with chemical exchange saturation transfer (CEST).[51] This technique takes advantage of the exchange of hp ^{129}Xe between the cryptophane interior and bulk solvent. By applying radiofrequency saturation pulses that are selective to the cryptophane-bound ^{129}Xe population, the cryptophane

can be indirectly detected by monitoring the subsequent loss of aqueous ^{129}Xe NMR signal. Ultrasensitive (nM-to-fM) detection of protein gas vesicles,[52] bacterial spores,[53] nanoemulsion droplets,[54] and water-soluble small-molecule hosts has been achieved using the hyper-CEST NMR technique.[43,55–57]

In order to harness the enhanced detection sensitivity of hyper-CEST NMR/MRI, we and others have sought to optimize the design of cryptophane-based biosensors.[58,59] We previously synthesized biosensor C8B (Figure 1) and investigated its interaction with target carbonic anhydrase II (CAII), a cytoplasmic CA isozyme important in carbon dioxide transport and pH regulation in healthy cells.[37,60] A crystal structure of the C8B-CAII complex confirmed coordination of the benzenesulfonamidate ligand to the Zn(II) active site.[61] However, ambiguous ^{129}Xe NMR peak assignments[37,62] compelled us to reinvestigate C8B binding to CAII and extend this analysis to the catalytic domain of CAXII, a membrane-bound CA isozyme upregulated in many cancers.[63] For comparison, we used the previously synthesized water-soluble tris(triazole propionic acid) cryptophane-A derivative (TTPC, Figure 1)[64] lacking a benzenesulfonamide CA-targeting moiety.

Many water-soluble cryptophanes and cryptophane-based xenon biosensors have been characterized using HPLC, ^{1}H/^{13}C/^{129}Xe NMR spectroscopy, and mass spectrometry to confirm purity and identity, and have been considered to be well-solvated, molecular species in aqueous solution. However, dynamic light scattering (DLS) and fluorescence assays revealed that C8B, TTPC, and other water-soluble cryptophanes at low micromolar concentrations are not monomeric molecules in aqueous solution, as generally assumed, but instead form water-soluble aggregates that are tens-to-hundreds of nanometers in size. C8B becomes monomeric upon binding to target CA protein, consistent with our previous X-ray crystal structure[61] as well as ITC measurements showing stoichiometric C8B-CA binding.[37] Ultrasensitive hyper-CEST ^{129}Xe NMR spectroscopy enables investigation of Xe-cryptophane behavior at concentrations where cryptophane is either monomeric (nM) or aggregated (μM). These studies provide new insight into the solution-phase behavior of cryptophanes and cryptophane-based biosensors, and offer important considerations for evaluating their xenon-binding and biosensing characteristics.

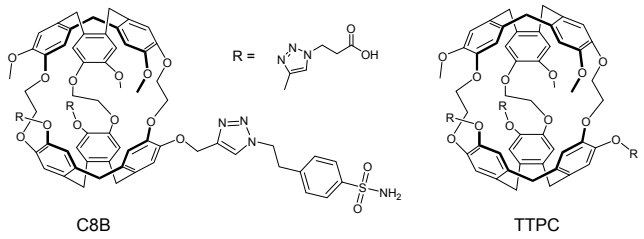

Figure 1. Molecular structures of biosensor C8B and water-soluble cryptophane TTPC. The benzenesulfonamide moiety of C8B coordinates to Zn^{2+} in the active site of CA.

EXPERIMENTAL SECTION

Synthetic methods. TTPC and C8B were synthesized from the precursor tripropargyl cryptophane, which was synthesized as described previously *via* a 6-step non-linear synthesis. The spectroscopic data match those reported in the literature.[43] Three azidopropionic acid solubilizing groups were appended to tripropargyl cryptophane *via* copper(I)-catalyzed [3 + 2] azide-alkyne cycloaddition to generate TTPC as described previously. The spectroscopic data match those reported in the literature.[64] Two azidopropionic acid solubilizing groups and one benzenesulfonamide linker were similarly appended to tripropargyl cryptophane to generate C8B as described previously. The spectroscopic data match those reported in the literature.[37] To synthesize TAAC, the propargyl moieties of tripropargyl cryptophane were first removed to give trihydroxy cryptophane, as described previously.[65] TAAC was then synthesized from trihydroxy cryptophane in a 2-step synthesis. The spectroscopic data match those reported in the literature.[66] Cryptophane-A was synthesized following previously described procedures. The spectroscopic data match those reported in the literature.[67]

CAII expression and purification. CAII was expressed and purified as described previously.[32] Briefly, a pCAM plasmid containing the full-length human CAII gene (UniProt accession no. P00918) was transformed into BL21(DE3) competent *E. coli* cells. Protein expression was induced with 1 mM isopropyl-β-D-thiogalactopyranoside (IPTG) in the presence of 1 mM $ZnSO_4$. Cells were lysed in 50 mM sodium phosphate (pH 7.4), 0.3 M NaCl, and the soluble fraction was purified by nickel immobilized-metal affinity chromatography followed by size-exclusion chromatography. Isothermal titration calorimetry experiments to characterize C8B-CAII binding were performed previously.[37]

CAXII expression and purification. A pET-20b(+) expression vector containing the sequence encoding the extracellular catalytic domain of human CAXII (UniProt accession no. O43570) was transformed into BL21(DE3) competent *E. coli* cells (New England Biolabs) and grown overnight at 37 °C on LB-agar culture plates containing 100 μg/mL ampicillin. Single colonies of transformed cells were used to inoculate 5 mL of LB media supplemented with 200 μg/mL ampicillin. The 5 mL starter cultures were incubated overnight at 37 °C with shaking at 250 rpm. The 5 mL cultures were used to inoculate 6 x 1 L of 2xYT media supplemented with 200 μg/mL ampicillin in baffled culture flasks. The 1 L cell cultures were incubated at 37 °C with shaking at 250 rpm until OD_{600} reached ~1. Protein expression was induced by adding IPTG to a final concentration of 1 mM and $ZnSO_4$ to a final concentration of 1 mM. The induced cultures were incubated overnight at 25 °C with shaking at 250 rpm. The cells were pelleted by centrifugation and frozen at -80 °C for long-term storage.

The frozen cell pellet was thawed in 50 mM sodium phosphate (pH 7.4), 0.3 M NaCl and stirred at rt until the cell suspension was homogeneous. The cells were lysed with lysozyme (Sigma) and DNAse was added to the lysate to reduce viscosity. The lysate was clarified and the insoluble fraction containing CAXII inclusion bodies was washed with 50 mM sodium phosphate (pH 7.4), 0.3 M NaCl, 2 M urea, 1% (v/v) Triton X-100, rinsed with 50 mM sodium phosphate (pH 7.4), 0.3 M NaCl, and then resuspended in 50 mM sodium phosphate (pH 7.4), 0.3 M NaCl, 8 M urea, 5-20 mM BME. CAXII was refolded *via* snap dilution by adding unfolded CAXII dropwise into rt 50 mM Tris (pH 8.0), 2 mM reduced glutathione, 0.2 mM oxidized glutathione, 5-7 μM $ZnSO_4$, and 10% (v/v) glycerol with rapid stirring. Refolded CAXII was loaded onto a 5 mL Q HP anion-exchange column (GE Healthcare) pre-equilibrated with 50 mM Tris (pH 8.0), 10% (v/v) glycerol and eluted *via* a gradient to 50 mM Tris (pH 8.0), 10% (v/v)

glycerol, 3 M NaCl. The eluted fractions were evaluated by SDS-PAGE, and fractions containing pure CAXII were pooled, concentrated, and then loaded onto a HiLoad 16/600 Superdex size-exclusion column (GE Healthcare Life Sciences) pre-equilibrated with 50 mM Tris (pH 8.0), 10% (v/v) glycerol. Eluted fractions containing pure CAXII were pooled, and analysis by SDS-PAGE indicated that the protein was over 95% pure. Protein concentration was determined by measuring absorbance at 280 nm using the extinction coefficient (ε_{280} = 42985 M^{-1} cm^{-1}) calculated by the PROTPARAM server.[68]

Isothermal titration calorimetry (ITC) with CAXII and C8B. All ITC experiments were performed in triplicate at 298 K on a GE Healthcare MicroCal™ iTC200 instrument. Ligands were prepared at concentrations of 300-345 μM in 50 mM Tris (pH 8.0), 10% (v/v) glycerol, 3% (v/v) DMSO. CAXII was diluted to 30 μM in 50 mM Tris (pH 8.0), 10% (v/v) glycerol) and DMSO was added to match the final composition of the ligand solution. Prior to performing ITC, both the ligand and protein solutions were degassed by brief bath sonication followed by centrifugation at 13.4k rpm for 5 min. The sample cell was filled with 300 μL of CAXII solution, and the reference cell was filled with water. Calorimetric data were analyzed by performing nonlinear regression fitting to the binding isotherm using ORIGIN software. The data are shown in Table S1 and Figure S1.

Dynamic light scattering (DLS). Samples were prepared as 100 μM cryptophane in pH 7.2 PBS buffer with 0.1% DMSO. Samples were filtered *via* 0.22 μm centrifugal filter units. The temperature was set to 298 K. The number and intensity distributions were analyzed. Measurements were averaged over 3 trials. DLS data were collected on the Zetasizer Nano Z system, using software from Malvern Instruments Ltd. v. 2.0.

Determination of cryptophane monomeric to aggregated transition *via* fluorescence spectroscopy. This method was adapted from the literature.[69] A stock solution of 145.5 μM acridine orange (Sigma) in pH 7.2 PBS buffer was prepared. Care was taken to avoid light exposure to solutions containing acridine orange. Aliquots of 3.4 μL of this solution were added to 100 μL samples of cryptophane in pH 7.2 PBS buffer with 0.1% DMSO at varying concentrations. The acridine orange concentration was 4.8 μM for all samples. The acridine orange-cryptophane solution was mixed thoroughly before fluorescence measurements. The excitation wavelength was 436 nm. The PMT voltage was 900 V. Emission at 525 nm was monitored. Measurements were averaged over 3 trials. Fluorescence measurements were obtained using a Varian Cary Eclipse Fluorescence Spectrophotometer.

^{129}Xe NMR hyper-CEST frequency scans. Hyperpolarized (hp) ^{129}Xe was generated using the spin-exchange optical pumping (SEOP) method with a home-built ^{129}Xe polarizer based on the IGI.Xe.2000 commercial model by GE. A Shark 65 W tunable ultra-narrow band diode laser (OptiGrate) set to 795 nm was used for optical pumping of Rb vapor. A gas mixture of 88% helium, 10% nitrogen, and 2% natural abundance xenon (Linde Group, NJ) was used as the hyperpolarizer input. ^{129}Xe hyperpolarization level was roughly 10-15%. For each data point in the hyper-CEST z-spectra, hp ^{129}Xe was bubbled into a 10-mm NMR tube containing 2.5 mL of sample through capillaries for 20 s, followed by a 3-s delay to allow bubbles to collapse. A Dsnob saturation pulse with 690 Hz bandwidth was used. Pulse length t_{pulse} = 3.80 ms, field strength $B_{1,max}$ = 77 μT, number of pulses n_{pulse} = 400, saturation time T_{sat} = 1.52 s. NMR experiments were performed using a Bruker BioDRX 500 MHz NMR spectrometer and a 10-mm PABBO probe at 300 K. A 90° hard pulse of this probe has a pulse length of 22 μs. For all experiments, the cryptophane and/or protein concentration was 5 μM, in pH 7.2 PBS, with 0.1% DMSO and 0.1% (v/v) Pluronic L81 (Aldrich) to mitigate foaming. Measurements were averaged over 3 trials.

^{129}Xe NMR hyper-CEST depolarization curves. For C8B only, saturation frequencies of Dsnob shaped pulses were positioned at (193 – 130) = 63 ppm for on resonance and (193 + 130) = 323 ppm for off resonance. For 1:5 C8B:CAII samples, pulses were positioned at (193 – 124) = 69 ppm for on-resonance and (193 + 124) = 317 ppm for off-resonance. In each experiment, the following parameters were used: Pulse length t_{pulse} = 2.624 ms, field strength $B_{1,max}$ = 112 μT, delay between pulses = 20 μs, maximum number of saturation cycles = 10 000 for 100 nM C8B and 5 000 for 1 μM C8B. Measurements were averaged over 3 trials.

Direct detection hp ^{129}Xe NMR spectroscopy of C8B-CAXII sample. Hp ^{129}Xe was cryogenically separated, accumulated, thawed, and collected in controlled atmosphere valve 5 mm NMR tubes (New Era). Prior to data collection, tubes were vigorously shaken to mix sample solutions with Xe. NMR experiments were performed using a Bruker BioDRX 500 MHz NMR spectrometer and a 5-mm BBO probe at 300 K. A selective pulse centered at 66 ppm with excitation bandwidth of 2000 Hz was used, and signal averaged over 16 scans. Fourier-transformed spectra were processed with zero-filling and Lorentzian line broadening of 20 Hz. Chemical shifts were referenced to aqueous ^{129}Xe at 197.6 ppm.

RESULTS AND DISCUSSION

DLS measurements of cryptophane solutions. Figure 2 shows the size distribution measurements obtained by DLS for solutions in pH 7.2 PBS of biosensor C8B with and without CA target, and in comparison to TTPC. It was observed that on its own, 100 μM C8B was aggregated in solution, with an average diameter of 345 ± 13 nm, considerably larger than expected for a ~1 nm diameter molecule. When equimolar CAII was added to 100 μM C8B (apparent K_d = 60 ± 20 nM, measured by ITC at 298 K),[37] the complex exhibited a narrower size distribution with an average diameter of 4.4 ± 0.1 nm, which is approximately the expected diameter of CAII,[61,70] and just 0.8 nm larger than the average diameter of CAII alone in solution (for the corresponding DLS data, see Figure S1). This transition from aggregated to monomeric state was also observed in the binding of C8B to CAXII (Figure S1): ITC gave apparent K_d of 2.07 ± 0.03 μM at 298 K, Table S1, raw ITC data shown in Figure S2. By first incubating CAII with the high-affinity inhibitor acetazolamide (K_d = 7.5 nM),[70] C8B binding to CAII was blocked and the biosensor remained aggregated, with average diameter of 1000 ± 50 nm. This approximately 3-fold increase in average diameter from the 'C8B only' condition was likely due to nonspecific interactions between cryptophane and protein. Notably, this is relevant to many cellular applications, where nonspecific protein binding has the potential to stabilize larger cryptophane aggregates. The DLS-determined size distribution of TTPC (average diameter = 55 ± 5 nm, Figure 2) highlights that substituting the triazole-benzenesulfonamide targeting moiety of C8B with a third triazole-propioniate moiety reduced the average diameter

by approximately six-fold. It is likely that the shorter length of the propionate moiety, as well as its reduced hydrophobicity, disfavored formation of very large aggregates.

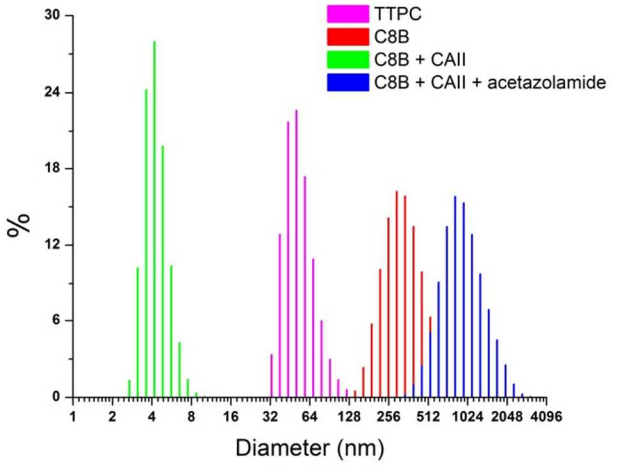

Figure 2. DLS data showing size distribution by number in pH 7.2 PBS with 0.1% DMSO at 298 K of 100 μM TTPC; average diameter = 55 ± 5 nm; PdI = 0.485, 100 μM C8B; average diameter = 345 ± 13 nm; PdI = 0.119, 100 μM C8B-CAII; average diameter = 4.4 ± 0.1 nm; PdI = 0.497, and 100 μM C8B-CAII + 500 μM acetazolamide; average diameter = 1000 ± 50 nm; PdI = 0.403.

By DLS, we also observed aggregation of the previously synthesized triacetic acid cryptophane-A derivative (TAAC)[66] (Figure S3), which supports our hypothesis that all cryptophanes, depending on concentration in solution, may exist in aggregated form. Notably, TTPC was also determined using DLS to aggregate in the organic solvent dimethylformamide (DMF) (average diameter = 70 ± 5 nm, Figure S4), indicating a general self-association phenomenon that goes beyond the well-recognized challenge of solvating cryptophane in aqueous solution. Aggregation of cryptophane-A in DMF was observed to a lesser extent (average diameter = 13.2 ± 0.4 nm, Figure S5), suggesting that functionalization of the cryptophane cage may facilitate aggregation. Interestingly, this aggregation behavior is not seen with cucurbit[6]uril (CB[6]), a commercially available Xe-binding macrocycle[71] that has been similarly shown to be an ultrasensitive ^{129}Xe NMR contrast agent using hyper-CEST[56] and has been detected within the vasculature of a living rat.[72] Indeed, the DLS-determined size distribution of 100 μM CB[6] in pH 7.2 PBS is very narrow, with average diameter of 0.68 ± 0.01 nm (Figure S2). The apparent lack of CB[6] aggregation suggests that phenyl-phenyl π-stacking interactions may promote aggregation in cryptophanes, although the molecular features underpinning this phenomenon are still under investigation.

A single xenon atom can occupy the cryptophane interior, as we established previously by small-molecule X-ray crystallography.[73] However, the clustering of cryptophanes into supramolecular aggregates suggests a role for additional "xenon-cryptophane interactions" in solution. For example, cryptophane clusters likely contain hydrophobic void spaces where many xenon atoms can reside, as has been observed in zeolites and, more recently, in porous organic cages.[74] Undoubtedly, in addition to the two conventionally assigned pools of xenon, one in bulk solvent and one bound to the tailored cryptophane cavity, there exists a third, less well-defined pool of xenon atoms contained in the larger cavities and pores within cryptophane clusters. Due to rapid exchange between these sites, solution ^{129}Xe NMR studies have not yet revealed these interactions. Nonetheless, pooling of xenon in close proximity to a cryptophane cavity should increase the apparent cryptophane-xenon affinity, as such host-guest interactions in supramolecular complexes are modulated by the size, chemical environment internal composition of the aggregate, including counterions.[75] This complicates efforts to measure cryptophane-Xe affinity, and we consider that Xe affinities that have been measured to date should be categorized as "apparent" dissociation constants. We will explore issues of Xe affinity in a follow-up work. Here, we consider that the formation of stable cryptophane biosensor aggregates can compete with the formation of the desired biosensor-target complex. Importantly, this realization can explain the observation of both "free" and "bound" peaks in prior hp ^{129}Xe NMR experiments, at concentrations and stoichiometries where only "bound" biosensor-protein peak was expected.

Concentration dependence of cryptophane aggregation state. A common method for determining the critical micelle concentration (CMC) of surfactant molecules involves the addition of a fluorescent dye to the surfactant solution, and monitoring fluorescence as a function of surfactant concentration.[69,76] As surfactant concentrations reach and exceed the CMC, the dye becomes adsorbed onto the micelles, and its fluorescence intensity decreases *via* static quenching resulting from high local concentrations of dye. Here, we used a similar method to determine the critical concentration at which amphiphilic cryptophanes transition from being monomeric to aggregated using the fluorescent dye acridine orange (AO). Figure 3 shows the percentage decrease in AO fluorescence at various concentrations of cryptophane in solution. Fitting these S-shaped (sigmoidal) data to a logistic growth curve allowed for the extraction of the critical concentration, which was found to be 201 ± 9 nM for TTPC and 601 ± 13 nM for C8B. It is striking that this transition point occurs at three-fold higher concentration for C8B than TTPC, given that C8B aggregates have an average diameter that is six-fold larger than those of TTPC. We hypothesize that the final size of these aggregates is unrelated to the minimum concentration necessary for aggregate nucleation. For instance, the high symmetry of TTPC may facilitate aggregation with its three identical solubilizing groups promoting interactions between neighboring TTPC molecules. In the case of C8B, the longer benzenesulfonamide linker may prevent initial aggregation at low concentrations due to steric effects. At higher concentrations, the benzenesulfonamide moiety may provide a hydrophobic scaffold that stabilizes larger aggregates. We note that the optical properties of these water-soluble aggregates obey the linear relationship between absorbance and concentration as described by the Beer-Lambert law. The absorbance of solutions of C8B in the concentration range of 1.6 – 85.6 μM was linearly proportional (R^2 = 0.994) to the concentration of the solutions (Figure S6). Indeed, the well-behaved solution properties of cryptophanes have long masked their supramolecular-aggregation behavior.

The aggregation behavior of biosensors in solution is an important consideration for *in vivo* applications. Biosensor aggregation may be a useful attribute for *in vivo* studies, for example, by increasing circulation time and improving biotargeting. Thus, it is important to study cryptophane biosen-

sors in solutions with the same physico-chemical properties (i.e., ionic strength, pH, viscosity, temperature) as the target biological fluid(s). It is also critical to study the solution behavior of xenon biosensors at the relevant concentrations of biosensor and protein target. HP ^{129}Xe NMR studies have been employed by several laboratories to identify biosensor-protein interactions based on changes in the cryptophane-^{129}Xe NMR chemical shift. Most of these studies have been performed via "direct detection" experiments where hp ^{129}Xe is bubbled into the biosensor-protein solution, and separate peaks are observed for ^{129}Xe in water and ^{129}Xe residing in cryptophane that is either "protein-bound" or "free". However, direct detection ^{129}Xe NMR experiments typically require high cryptophane concentration (~100 μM), where we have evidence the biosensor is strongly aggregated. These conditions also make it more difficult to work with super-stoichiometric concentrations of target biomolecule. Here, we employed the hyper-CEST ^{129}Xe NMR technique to examine xenon biosensor behavior over a wide range of concentrations (nM–μM) where the biosensor is either monomeric or aggregated. This facilitated the study of target-bound biosensor, as a function of increasing target concentration.

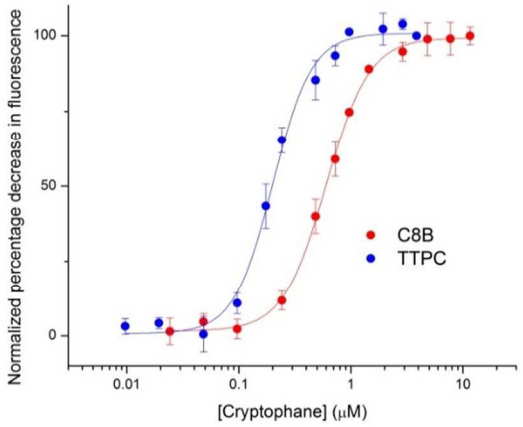

Figure 3. Percentage decrease in fluorescence emission at 525 nm of 4.8 μM acridine orange in pH 7.2 PBS with 0.1% DMSO at 298 K as a function of cryptophane concentration (λ_{ex} = 436 nm). Data were fitted to logistic growth curves to extract critical concentration values of 201 ± 9 nM and 601 ± 13 nM for TTPC and C8B, respectively.

^{129}Xe Hyper-CEST NMR with C8B and C8B-CA complexes. DLS results (Figure 2) established that C8B transitions from an aggregated to a monomeric state upon binding target biomolecule. C8B shares high structural similarity with the other published xenon biosensors, which opens many ^{129}Xe NMR studies to possible reinterpretation. In the original model, the change in ^{129}Xe-biosensor NMR chemical shift was proposed to result from protein-mediated mechanical distortion of the cryptophane, which is communicated to the bound xenon atom.[34,77–79] However, the observation of large cryptophane aggregates raises the possibility of a different model-mechanism where the ^{129}Xe NMR chemical shift change is a result of xenon transitioning from a hydrophobic cryptophane cluster to a monomeric, solvent-exposed cryptophane during target binding. In this model, it is possible that the protein target serves as a "disaggregase" but plays no direct role in perturbing the bound cryptophane nor the ^{129}Xe NMR chemical shift.

To investigate these competing models at a lower biosensor concentration where protein target can be supplied in large excess, we used the hyper-CEST NMR technique. First, we acquired ^{129}Xe hyper-CEST z-spectra with 5 μM C8B (Table 1). Upon addition of 5 μM CAII, the Xe@C8B-CAII peak shifted 3.9 ppm downfield from 62.6 ppm (C8B only) to 66.5 ppm, which is in good agreement with our previously published direct detection ^{129}Xe NMR results for the 1:1 complex.[37] Remarkably, when the C8B:CAII ratio was increased to 1:2, the Xe@C8B-CAII peak shifted further downfield to 68.2 ppm. Increasing this ratio to 1:5 or higher resulted in a maximum chemical shift of 68.5 ppm. Repeating these studies with the C8B-CAXII complex revealed a more gradual increase in the chemical shift of the Xe@C8B-CAXII peak (Table 1). Upon addition of 5 μM CAXII, the Xe@C8B-CAXII peak shifted only 1.0 ppm downfield from C8B only, which is in agreement with our direct detection ^{129}Xe NMR spectrum of C8B-CAXII at a 1:1 ratio (Figure S7). A 1:10 C8B:CAXII ratio was necessary to reach the maximum chemical shift of 65.3 ppm, within error. The z-spectra for these experiments are shown in Figure S8, and summarized in Table 1.

Table 1. Chemical shifts of ^{129}Xe encapsulated by C8B-CAII and C8B-CAXII complexes[a]

[protein] (μM)	Xe@C8B-CAII chemical shift (ppm)	Xe@C8B-CAXII chemical shift (ppm)
0	62.6 ± 0.3	62.6 ± 0.3
5	66.5 ± 0.2	63.6 ± 0.4
10	68.2 ± 0.3	64.1 ± 0.3
25	68.5 ± 0.3	64.8 ± 0.3
50	68.5 ± 0.3	65.2 ± 0.3
100	68.5 ± 0.4	65.3 ± 0.2

[a] Performed at varying concentrations of protein in pH 7.2 PBS with 0.1% DMSO at 300 K. The C8B concentration was kept constant at 5 μM.

We attribute the gradual increase in ^{129}Xe NMR chemical shift (Table 1) to the progressive disaggregation of cryptophane clusters as more CA target was added to solution. In our previously published direct detection ^{129}Xe NMR experiment[37] (conducted with 100 μM C8B and CAII), this was observed as a decrease in intensity of the ^{129}Xe@C8B peak, with concomitant increase in intensity of the ^{129}Xe@C8B-CAII peaks. However, in the hyper-CEST experiment, we observe an average of the 'free' and 'bound' peaks and the resultant downfield chemical shift as the Xe@C8B-CAII population increases. Indeed, we see evidence by DLS of the presence of both C8B and C8B-CAII at a 1:1 C8B:CAII ratio when looking at the intensity distribution of particles, which shows all of the species present in solution (Figure S9), not just the dominant species as shown by the number distribution data in Figure 2.

We hypothesize that the difference in disaggregation behavior between the CAII and CAXII isozymes is due to the differing K_d values for the two C8B-CA complexes. The apparent K_d value ($K_{d(app)}$, Scheme 1) for the C8B-CAII complex, as measured by ITC (Figure S2), is 60 nM,[37] which is ~35-fold lower than that for the C8B-CAXII complex ($K_{d(app)}$ = 2.07 μM). This is consistent with the hyper-CEST results in Table 1, showing that more CAXII than CAII is necessary to dis-

aggregate C8B and form the stable protein complex. It is important to emphasize that the apparent K_d values measured by ITC for these complexes are indeed "apparent", due to the aggregated state of the cryptophane during these measurements. The equilibrium constant for the biosensor disaggregation-aggregation process (K_{d1}), which we measured by AO fluorescence quenching to be 601 nM (Figure 3), competes with the process of biosensor-CA dissociation-binding (K_{d2}), leading to an overall apparent K_d value, as measured by ITC (Scheme 1). This competition between two equilibrium processes involving the biosensor can be modeled most simply as $K_{d(app)} = \sqrt{[K_{d1} * K_{d2}]}$. Based on this simple model (which ignores the details of biosensor nanoparticle formation), we estimate that the K_{d2} value, reflecting the dissociation constant for monomeric cryptophane and CA target, is 6 nM for C8B-CAII and 7 μM for C8B-CAXII. A xenon biosensor that remains monomeric in solution (or a suitable solvent system), will facilitate testing of this binding model.

Scheme 1. Model for the competing processes of biosensor self-aggregation and biosensor-target binding.

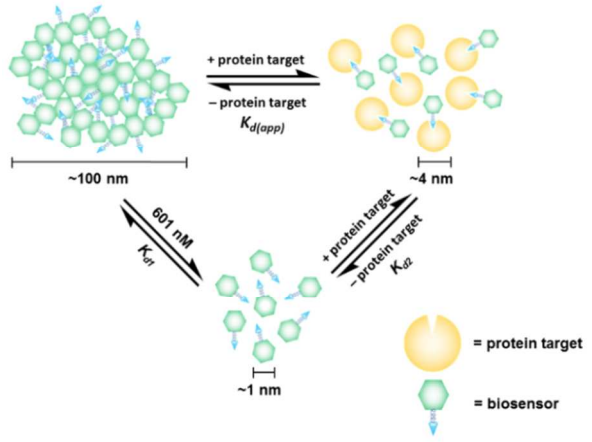

The difference in chemical shift of ^{129}Xe@C8B-CAII and ^{129}Xe@C8B-CAXII (δ = 3.2 ppm) at the 1:20 C8B:CA ratio (Table 1) supports the established biosensing model, where binding to a protein target perturbs the cryptophane, which is communicated to the bound ^{129}Xe atom. All C8B is bound as the stoichiometric protein complex at the 1:20 C8B:CA ratio. This protein-environmental (CAII vs. CAXII) chemical shift difference represents slightly more than half of the total chemical shift change observed for the C8B-CAII interaction (δ = 5.9 ppm) relative to free biosensor. Indeed, CAXII shares only 51% sequence homology with CAII. In particular, the side chains of residues 131-133, among others,[80] differ in the region occupied by the cryptophane (see Figure S10), which likely contributes to the observed differences in ^{129}Xe NMR chemical shift and affinity for the two C8B-CA complexes. The similarity between the "bound" (64.5 and 61.6 ppm) and "free" (63.1 ppm) peaks for C8B-CAXII in the direct detection NMR spectrum (Figure S7) suggests that there is relatively little interaction between the cryptophane and CAXII, consistent with the lower affinity for this isozyme. We conclude that the newly discovered cryptophane (dis)aggregation phenomenon contributes significantly to the observed ^{129}Xe NMR chemical shift change upon biosensor binding to CA. The ability to distinguish the cancer biomarker CAXII from cytoplasmic CAII using both direct detection and hyper-CEST ^{129}Xe NMR is another important finding in this study.

To compare the hyper-CEST detection sensitivity of biosensor alone to the biosensor-target complex, time-dependent saturation transfer experiments were performed by measuring the aqueous ^{129}Xe NMR signal as a function of saturation duration. The normalized difference between on- and off- resonance saturation transfer was reported as hyper-CEST saturation contrast. To ensure that the biosensor was completely protein-bound in the C8B-CA solution, a 1:5 C8B:CAII ratio was used. By this method, it was found that 100 nM C8B reported 0.22 ± 0.02 saturation contrast, and 100 nM C8B with 500 nM CAII reported 0.18 ± 0.02 saturation contrast (Figure S11). Notably, 100 nM C8B is monomeric in solution. The similarity in observed contrast between "free" and "bound" biosensor suggests that the target-bound state does not significantly affect the overall CEST efficiency of the biosensor.

To determine whether biosensor aggregation affects CEST efficiency, these experiments were repeated with 1 μM C8B, which is in mostly aggregated form (Figure 3). It was found that 1 μM C8B reported 0.48 ± 0.02 saturation contrast, whereas 1 μM C8B with 5 μM CAII reported 0.66 ± 0.03 saturation contrast (Figure S12). This 38% increase in contrast upon biosensor disaggregation suggests that Xe exchange is favored in the monomeric cryptophane species, likely due to greater Xe accessibility. It is important to note that CAII alone at 5 μM does not give any CEST response at this frequency (Figure S8a), indicating that the contrast enhancement is due exclusively to C8B disaggregation. This effect may be exploited for *in vivo* ^{129}Xe MR imaging experiments, as biosensor-target binding should produce significant enhancement of the CEST effect relative to aggregated biosensor. These predictions have been partially validated with cucurbit[6]uril, which remains monomeric and yields efficient hyper-CEST contrast in solution[56] and *in vivo*,[72] despite its modest xenon affinity.

CONCLUSIONS

In summary, we determined that cryptophane-A, the water-soluble cryptophanes TTPC and TAAC, and the cryptophane biosensor C8B form aggregates in solution with diameters of tens to hundreds of nanometers at rt. Fluorescence quenching assays with acridine orange identified the transition from monomeric to aggregated C8B biosensor at approximately 600 nM concentration. TTPC was more prone to aggregation, with critical concentration of ca. 200 nM. This indicates that cryptophane aggregates predominate in solution when performing routine ^{129}Xe NMR biosensing and xenon binding studies, as well as obtaining z-spectra *via* the hyper-CEST NMR technique, all of which typically employ micromolar cryptophane concentrations. The biosensor aggregation process appears to be fully reversible, with strong potential for disaggregation upon target binding. Hyper-CEST NMR experiments were performed at different ratios of C8B biosensor and CA isozymes II and XII, with the ^{129}Xe NMR chemical shift migrating 2.7 ppm downfield for the cancer biomarker CAXII and 5.9 ppm downfield for CAII. In both experiments, the biosensor aggregate was replaced with 1:1 biosensor-CA complex at higher ratios of CA protein. Finally, we found that biosensor disaggregation *via* target binding increased CEST efficiency by approximately 38%.

The propensity of cryptophanes to aggregate in solution has profound consequences for many ongoing cryptophane studies, including efforts to: (1) improve and/or measure cryptophane-Xe affinity, where only the molecular host-guest complex has been considered; (2) multiplex ^{129}Xe NMR signals from different cryptophanes in solution, where hetero-cryptophane aggregates may potentially form; and (3) assign interactions between cryptophane biosensors and target biomolecules to chemical shift changes observed by ^{129}Xe NMR spectroscopy. Our findings suggest that the chemical shift changes thought to result from cryptophane-mechanical perturbation by biological targets have an additional contribution from biosensor disaggregation. We consider that aggregation itself may be useful for many *in vivo* applications, as formation of "cryptophane nanoparticles" that are tens-to-hundreds of nanometers in size should extend the circulation time of cryptophane biosensors *in vivo*. Notably, these nanoparticles show propensity to increase to micron size *via* non-specific protein interaction.

The insights gleaned from DLS, AO fluorescence quenching, and hyper-CEST NMR characterization methods using two different CA isozymes provide a stronger foundation for developing cryptophane-based sensors. For example, cryptophane-based metal ion sensors[45–49] are likely to exhibit different aggregation states depending on the metal ion(s) in solution, which may contribute to the observed ^{129}Xe NMR chemical shift(s). Over the past decade, our laboratory and others have produced a variety of xenon-cryptophane biosensors; we hypothesize that all of these biosensors exist as aggregates at micromolar concentrations in solution. Many xenon biosensors have yielded only modest ^{129}Xe NMR chemical shift changes when bound to their targets.[35,36,40,45] This could result if the biosensor aggregate is more stable than the desired biosensor-target complex. In this scenario, experiments performed with stoichiometric biosensor and biomolecular target in solution will produce little of the desired biosensor-target complex. Biosensor disaggregation may result in modest ^{129}Xe NMR chemical shift change (as seen for C8B with CAXII), and in cases where target binding results in stereoelectronic perturbation of the cryptophane, additional ^{129}Xe NMR chemical shift changes should result (as observed for C8B with CAII, with support from X-ray crystallographic data[61]).

Cryptophane aggregation phenomena complicate the interpretation of many previous studies, but now provide a mechanism for modulating Xe-cryptophane interactions and potentially developing new classes of xenon-based sensors. For example, we recently described a "turn-on" xenon biosensor that produced no ^{129}Xe NMR signal until bound to its calmodulin target[30]—we hypothesize that biosensor aggregation coupled with peptide-cryptophane interactions produced this particular "off" state. With a new understanding of cryptophane solution behavior, this is a critical juncture to reevaluate the methods used in the synthesis, purification, and characterization of these compounds, as well as their application. Further investigation into the properties of these aggregates should allow for their optimization and control, as has previously been achieved with similar supramolecular constructs.[5,8,9,14] Finally, we expect that many other drug-like molecules form water-soluble aggregates that have similarly escaped detection, and such nanoscale assemblies (perhaps stabilized by a protein corona) have the potential to modulate *in vivo* stability, circulation, cell transport, and target binding, among other properties.

ASSOCIATED CONTENT

Supporting Information

The Supporting Information is available free of charge on the ACS Publications website at DOI: [insert DOI here].

ITC, DLS, UV-Vis, direct detection and hyper-CEST ^{129}Xe NMR data, and modeling of protein-cryptophane interaction (PDF)

AUTHOR INFORMATION

Corresponding Author

Email: ivandmo@sas.upenn.edu

Present Addresses

† Netter Center for Community Partnerships, 111 S 38th St, Philadelphia, PA 19104

‡ Harvard Medical School, 25 Shattuck St, Boston, MA 02115

Notes

The authors declare no competing financial interest.

ACKNOWLEDGMENT

This work was supported by NIH R01-GM097478. We thank the University of Pennsylvania Chemistry NMR facility for spectrometer time and Yannan Lin for synthesizing pure cryptophane-A and determining the size distribution in DMF. We remember Dr. George Furst for his kind support and many years of service.

REFERENCES

(1) Janiak, J.; Tomšič, M.; Lundberg, D.; Olofsson, G.; Piculell, L.; Schillén, K. *J. Phys. Chem. B* **2014**, *118* (32), 9745.

(2) Mani, G.; Kyobum, K.; Sengottuvelan, B. *Sci. Rep.* **2017**, *7* (1), 1.

(3) Esparza, T. J.; Wildburger, N. C.; Jiang, H.; Gangolli, M.; Cairns, N. J.; Bateman, R. J.; Brody, D. L. *Sci. Rep.* **2016**, *6*, 1.

(4) Ohno, O.; Kaizu, Y.; Kobayashi, H. *J. Chem. Phys.* **1993**, *99* (5), 4128.

(5) Roux, M.; Perly, B.; Djedaïni-Pilard, F. *Eur. Biophys. J.* **2007**, *36* (8), 861.

(6) Chan, J. M. W.; Tischler, J. R.; Kooi, S. E.; Bulovic, V.; Swager, T. M. *J. Am. Chem. Soc.* **2009**, *131* (15), 5659.

(7) Avilova, I. A.; Chernyak, A. V.; Zhilenkov, A. V.; Troshin, P. A.; Volkov, V. I. *Mendeleev Commun.* **2016**, *26* (2), 146.

(8) Challa, R.; Ahuja, A.; Ali, J.; Khar, R. K. *AAPS PharmSciTech* **2005**, *6* (2), E329.

(9) Uekama, K. *Chem. Pharm. Bull.* **2004**, *52* (8), 900.

(10) Lahiani-Skiba, M.; Bounoure, F.; Shawky-Tous, S.; Arnaud, P.; Skiba, M. *J. Pharm. Biomed. Anal.* **2006**, *41* (3), 1017.

(11) Memisoglu-Bilensoy, E.; Vural, I.; Bochot, A.; Renoir, J. M.; Duchene, D.; Hincal, A. A. *J. Control. Release* **2005**, *104* (3), 489.

(12) Schmitt, C.; Bovay, C.; Rouvet, M.; Shojaei-Rami, S.; Kolodziejczyk, E. *Langmuir* **2007**, *23* (8), 4155.

(13) Ryan, K. N.; Zhong, Q.; Foegeding, E. A. *J. Food Sci.* **2013**, *78* (8), R1105.

(14) Wang, J.; Mei, J.; Hu, R.; Sun, J. Z.; Qin, A.; Tang, B. Z. *J. Am. Chem. Soc.* **2012**, *134* (24), 9956.

(15) Zhao, Z.; Chen, S.; Shen, X.; Mahtab, F.; Yu, Y.; Lu, P.; Lam, J. W. Y.; Kwok, H. S.; Tang, B. Z. *Chem. Commun.* **2010**, *46* (5), 686.

(16) Luo, J.; Xie, Z.; Lam, J. W. Y.; Cheng, L.; Tang, B. Z.; Chen, H.; Qiu, C.; Kwok, H. S.; Zhan, X.; Liu, Y.; Zhu, D. *Chem. Commun.* **2001**, *381* (18), 1740.

(17) Kumar, S.; Singh, P.; Mahajan, A.; Kumar, S. *Org. Lett.* **2013**, *15* (13), 3400.

(18) Liu, Y.; Nie, J.; Niu, J.; Meng, F.; Lin, W. *Sci. Rep.* **2017**, *7* (1), 1.

(19) Canceill, J.; Lacombe, L.; Collet, A. *J. Am. Chem. Soc.* **1985**, *107* (24), 7093.

(20) Brotin, T.; Dutasta, J.-P. *Chem. Rev.* **2009**, *109* (1), 88.

(21) Bartik, K.; Luhmer, M.; Dutasta, J. P.; Collet, A.; Reisse, J. *J. Am. Chem. Soc.* **1998**, *120* (4), 784.

(22) Matin, T. N.; Rahman, N.; Nickol, A. H.; Chen, M.; Xu, X.; Stewart, N. J.; Doel, T.; Grau, V.; Wild, J. M.; Gleeson, F. V. *Radiology*. **2017**, *282* (3), 857.

(23) Rao, M. R.; Stewart, N. J.; Griffiths, P. D.; Norquay, G.; Wild, J. M. *Radiology*. **2018**, *286* (2) 659.

(24) Rao, M.; Stewart, N. J.; Norquay, G.; Griffiths, P. D.; Wild, J. M. *Magn. Reson. Med.* **2016**, *75* (6), 2227.

(25) Ruan, W.; Zhong, J.; Han, Y.; Sun, X.; Ye, C.; Zhou, X.; Wang, K.; Wu, G. *J. Magn. Reson. Imaging*. **2017**, *45* (3), 879.

(26) Haynes, W. M. *CRC Handbook of Chemistry and Physics, 79th ed.*; CRC Press: Boca Raton, 2012.

(27) Clever, H. L. *Krypton, Xenon and Radon - Gas Solubilities*; Pergamon Press: New York, 1979.

(28) Raftery, D. *Annu. reports NMR Spectrosc.* **2006**, *57* (205), 205.

(29) Barskiy, D. A.; Coffey, A. M.; Nikolaou, P.; Mikhaylov, D. M.; Goodson, B. M.; Branca, R. T.; Lu, G. J.; Shapiro, M. G.; Telkki, V. V.; Zhivonitko, V. V.; Koptyug, I. V.; Salnikov, O. G.; Kovtunov, K. V.; Bukhtiyarov, V. I.; Rosen, M. S.; Barlow, M. J.; Safavi, S.; Hall, I. P.; Schröder, L.; Chekmenev, E. Y. *Chem. - A Eur. J.* **2017**, *23* (4), 725.

(30) Riggle, B. A.; Greenberg, M. L.; Wang, Y.; Wissner, R. F.; Zemerov, S. D.; Petersson, J.; Dmochowski, I. J. *Org. Biomol. Chem.* **2017**, *15*, 8883.

(31) Roose, B. W.; Zemerov, S. D.; Dmochowski, I. J. *Chem. Sci.* **2017**, *8*, 7631.

(32) Wang, Y.; Roose, B. W.; Philbin, J. P.; Doman, J. L.; Dmochowski, I. J. *Angew. Chem. Int. Ed.* **2016**, *55* (5), 1733.

(33) Finbloom, J. A.; Slack, C. C.; Bruns, C. J.; Jeong, K.; Wemmer, D. E.; Pines, A.; Francis, M. B. *Chem. Commun.* **2016**, *52* (15), 3119.

(34) Spence, M. M.; Rubin, S. M.; Dimitrov, I. E.; Ruiz, E. J.; Wemmer, D. E.; Pines, A.; Yao, S. Q.; Tian, F.; Schultz, P. G. *Proc. Natl. Acad. Sci.* **2001**, *98* (19), 10654.

(35) Wei, Q.; Seward, G. K.; Hill, P. A.; Patton, B.; Dimitrov, I. E.; Kuzma, N. N.; Dmochowski, I. J. *J. Am. Chem. Soc.* **2006**, *128* (40), 13274.

(36) Khan, N. S.; Riggle, B. A.; Seward, G. K.; Bai, Y.; Dmochowski, I. J. *Bioconjugate Chem.* **2015**, *26* (1), 101.

(37) Chambers, J. M.; Hill, P. A.; Aaron, J. A.; Han, Z.; Christianson, D. W.; Kuzma, N. N.; Dmochowski, I. J. *J. Am. Chem. Soc.* **2009**, *131* (2), 563.

(38) Seward, G. K.; Bai, Y.; Khan, N. S.; Dmochowski, I. J. *Chem. Sci.* **2011**, *2* (6), 1103.

(39) Kotera, N.; Dubost, E.; Milanole, G.; Doris, E.; Gravel, E.; Arhel, N.; Brotin, T.; Dutasta, J.-P.; Cochrane, J.; Mari, E.; Boutin, C.; Leonce, E.; Berthault, P.; Rousseau, B. *Chem. Commun.* **2015**, *51* (57), 11482.

(40) Schlundt, A.; Kilian, W.; Beyermann, M.; Sticht, J.; Günther, S.; Höpner, S.; Falk, K.; Roetzschke, O.; Mitschang, L.; Freund, C. *Angew. Chem. Int. Ed.* **2009**, *48* (23), 4142.

(41) Boutin, C.; Stopin, A.; Lenda, F.; Brotin, T.; Dutasta, J.-P.; Jamin, N.; Sanson, A.; Boulard, Y.; Leteurtre, F.; Huber, G.; Bogaert-Buchmann, A.; Tassali, N.; Desvaux, H.; Carrière, M.; Berthault, P. *Bioorg. Med. Chem.* **2011**, *19* (13), 4135.

(42) Yang, S.; Jiang, W.; Ren, L.; Yuan, Y.; Zhang, B.; Luo, Q.; Guo, Q.; Bouchard, L.-S.; Liu, M.; Zhou, X. *Anal. Chem.* **2016**, *88* (11), 5835.

(43) Riggle, B. A.; Wang, Y.; Dmochowski, I. J. *J. Am. Chem. Soc.* **2015**, *137* (16), 5542.

(44) Berthault, P.; Desvaux, H.; Wendlinger, T.; Gyejacquot, M.; Stopin, A.; Brotin, T.; Dutasta, J.-P.; Boulard, Y. *Chem. - A Eur. J.* **2010**, *16* (43), 12941.

(45) Guo, Q.; Zeng, Q.; Jiang, W.; Zhang, X.; Luo, Q.; Zhang, X.; Bouchard, L.-S.; Liu, M.; Zhou, X. *Chem. - A Eur. J.* **2016**, *22* (12), 3967.

(46) Jeong, K.; Slack, C. C.; Vassiliou, C. C.; Dao, P.; Gomes, M. D.; Kennedy, D. J.; Truxal, A. E.; Sperling, L. J.; Francis, M. B.; Wemmer, D. E.; Pines, A. *ChemPhysChem* **2015**, *16* (17), 3573.

(47) Kotera, N.; Tassali, N.; Léonce, E.; Boutin, C.; Berthault, P.; Brotin, T.; Dutasta, J.-P.; Delacour, L.; Traoré, T.; Buisson, D. A.; Taran, F.; Coudert, S.; Rousseau, B. *Angew. Chem. Int. Ed.* **2012**, *51* (17), 4100.

(48) Tassali, N.; Kotera, N.; Boutin, C.; Léonce, E.; Boulard, Y.; Rousseau, B.; Dubost, E.; Taran, F.; Brotin, T.; Dutasta, J.-P.; Berthault, P. *Anal. Chem.* **2014**, *86* (3), 1783.

(49) Zhang, J.; Jiang, W.; Luo, Q.; Zhang, X.; Guo, Q.; Liu, M.; Zhou, X. *Talanta* **2014**, *122*, 101.

(50) Roy, V.; Brotin, T.; Dutasta, J.-P.; Charles, M. H.; Delair, T.; Mallet, F.; Huber, G.; Desvaux, H.; Boulard, Y.; Berthault, P. *ChemPhysChem* **2007**, *8* (14), 2082.

(51) Lowery, T. J.; Hilty, C.; Wemmer, D. E.; Pines, A.; Schröder, L. *Science.* **2006**, *314* (5798), 446.

(52) Shapiro, M. G.; Ramirez, R. M.; Sperling, L. J.; Sun, G.; Sun, J.; Pines, A.; Schaffer, D. V.; Bajaj, V. S. *Nat. Chem.* **2014**, *6* (7), 629.

(53) Bai, Y.; Wang, Y.; Goulian, M.; Driks, A.; Dmochowski, I. J. *Chem. Sci.* **2014**, *5* (8), 3197.

(54) Stevens, T. K.; Ramirez, R. M.; Pines, A. *J. Am. Chem. Soc.* **2013**, *135* (26), 9576.

(55) Bai, Y.; Hill, P. A.; Dmochowski, I. J. *Anal. Chem.* **2012**, *84* (22), 9935.

(56) Wang, Y.; Dmochowski, I. J. *Chem. Commun.* **2015**, *51* (43), 8982.

(57) Kunth, M.; Döpfert, J.; Witte, C.; Rossella, F.; Schröder, L. *Angew. Chemie - Int. Ed.* **2012**, *51* (33), 8217.

(58) Wang, Y.; Dmochowski, I. J. *Acc. Chem. Res.* **2016**, *49* (10), 2179.

(59) Taratula, O.; Dmochowski, I. J. *Curr. Opin. Chem. Biol.* **2010**, *14* (1), 97.

(60) Supuran, C. T.; Scozzafava, A. *Bioorg. Med. Chem.* **2007**, *15* (13), 4336.

(61) Aaron, J. A.; Chambers, J. M.; Jude, K. M.; Costanzo, L. Di; Dmochowski, I. J.; Christianson, D. W. *J. Am. Chem. Soc.* **2008**, *130* (22), 6942.

(62) Taratula, O.; Bai, Y.; D'Antonio, E. L.; Dmochowski, I. J. *Supramol. Chem.* **2015**, *27* (1–2), 65.

(63) Supuran, C. T. *Nat. Rev. Drug Discov.* **2008**, *7* (2), 168.

(64) Hill, P. A.; Wei, Q.; Eckenhoff, R. G.; Dmochowski, I. J. *J. Am. Chem. Soc.* **2007**, *129* (30), 9262.

(65) Taratula, O.; Hill, P. A.; Bai, Y.; Khan, N. S.; Dmochowski, I. J. *Org. Lett.* **2011**, *13* (6), 1414.

(66) Hill, P. A.; Wei, Q.; Troxler, T.; Dmochowski, I. J. *J. Am. Chem. Soc.* **2009**, *131* (8), 3069.

(67) Benounis, M.; Jaffrezic-Renault, N.; Dutasta, J. P.; Cherif, K.; Abdelghani, A. *Sens. Actuator B-Chem.* **2005**, *107* (1), 32.

(68) Gasteiger, E.; Hoogland, C.; Gattiker, A.; Duvaud, S.; Wilkins, M. R.; Appel, R. D.; Bairoch, A. *The Proteomics Protocols Handbook*, Vol. 112.; Humana Press: Totowa, NJ, 2005.

(69) Rujimethanbhas, M.; Wilairat, P. *J. Chem. Educ.* **1978**, *55* (5), 342.

(70) Krishnamurthy, V. M.; Kaufman, G. K.; Urbach, A. R.; Gitlin, I.; L, K.; Weibel, D. B.; Whitesides, G. M. *Chem. Rev.* **2008**, *108* (3), 946.

(71) El Haouaj, M.; Luhmer, M.; Ko, Y. H.; Kim, K.; Bartik, K. *J. Chem. Soc. Perkin Trans. 2* **2001**, No. 5, 804.

(72) Hane, F. T.; Li, T.; Smylie, P.; Pellizzari, R. M.; Plata, J. A.; DeBoef, B.; Albert, M. S. *Sci. Rep.* **2017**, *7*, 41027.

(73) Taratula, O.; Hill, P. A.; Khan, N. S.; Carroll, P. J.; Dmochowski, I. J. *Nat. Commun.* **2010**, *1* (9), 148.

(74) Komulainen, S.; Roukala, J.; Zhivonitko, V. V.; Javed, M. A.; Chen, L.; Holden, D.; Hasell, T.; Cooper, A.; Lantto, P.; Telkki, V.-V. *Chem. Sci.* **2017**, No. 8, 5721.

(75) Davis, A. V; Yeh, R. M.; Raymond, K. N. *Proc. Natl. Acad. Sci. U. S. A.* **2002**, *99* (8), 4793.

(76) Roesslert, N. *J. Chem. Educ.* **1979**, *56* (10), 675.

(77) Spence, M. M.; Ruiz, E. J.; Rubin, S. M.; Lowery, T. J.; Winssinger, N.; Schultz, P. G.; Wemmer, D. E.; Pines, A. *J. Am. Chem. Soc.* **2004**, *126* (46), 15287.

(78) Lowery, T. J.; Garcia, S.; Chavez, L.; Ruiz, E. J.; Wu, T.; Brotin, T.; Dutasta, J.-P.; King, D. S.; Schultz, P. G.; Pines, A.; Wemmer, D. E. *ChemBioChem* **2006**, *7* (1), 65.

(79) Sears, D. N.; Jameson, C. J. *J. Chem. Phys.* **2003**, *119* (23), 12231.

(80) Whittington, D. A.; Waheed, A.; Ulmasov, B.; Shah, G. N.; Grubb, J. H.; Sly, W. S.; Christianson, D. W. *Proc. Natl. Acad. Sci. U. S. A.* **2001**, *98* (17), 9545.

For TOC only